Available online at www.sciencedirect.com
ScienceDirect
Acta Materialia 58 (2010) 5433–5442
Acta MATERIALIA
www.elsevier.com/locate/actamat

Strain glass in doped $Ti_{50}(Ni_{50-x}D_x)$ (D = Co, Cr, Mn) alloys: Implication for the generality of strain glass in defect-containing ferroelastic systems

Yumei Zhou [a,b], Dezhen Xue [a,b], Xiangdong Ding [a], Yu Wang [b], Jian Zhang [a], Zhen Zhang [a,b], Dong Wang [a], Kazuhiro Otsuka [a,b], Jun Sun [a], Xiaobing Ren [a,b,*]

[a] Multi-Disciplinary Materials Research Center, Frontier Institute of Science and Technology, State Key Laboratory for Mechanical Behavior of Materials, Xi'an Jiaotong University, Xi'an 710049, China
[b] Ferroic Physics Group, National Institute for Materials Science, Tsukuba 305-0047, Ibaraki, Japan

Received 26 February 2010; received in revised form 3 June 2010; accepted 8 June 2010
Available online 14 July 2010

Abstract

Strain glass is a new glassy state discovered recently in Ni-rich Ti–Ni ferroelastic alloys. However, it remains unclear whether or not strain glass can be found in a wide range of ferroelastic systems. Here, we investigated the transition behavior of three different defect-doped systems $Ti_{50}(Ni_{50-x}D_x)$ (D = Co, Cr, Mn) and found a striking similarity in their transition behavior as a function of defect concentration x. In all these systems, there exists a critical doping level x_c at which the transition behavior shows an interesting crossover. At $x < x_c$, these materials undergo a martensitic transition and the transition temperature decreases with increasing x. However, at $x > x_c$, the martensitic transition is suppressed and a strain glass transition occurs. These results imply that strain glass may be quite general in defect-containing ferroelastic systems. An analysis with a modified Landau-type free energy landscape suggests that although point defects always favor the formation of strain glass, to actually form a strain glass they need to destabilize the martensite of the system.

Keywords: Strain glass; Point defect; Generality; Local barrier; Martensitic transition

1. Introduction

Martensitic transition has attracted keen attention for decades, since it plays a key role in the shape memory effect (SME) and superelasticity (SE), which enables the wide applications of Ti–Ni alloys [1–7]. Recently, Ni-rich $Ti_{50-x}Ni_{50+x}$ ($x \geqslant 1.5$ at.%) alloys, known to undergo no martensitic transition, have been reported to undergo a "strain glass" transition, which is a new glassy state in ferroelastic systems [8]. This non-martensitic strain glass alloy also exhibits a novel SME and SE, based on the stress-induced strain glass to martensitic transition [9]. Strain glass significantly expands the regime of the SME and SE and may lead to new applications. However, so far strain glass has been reported only in two systems, $Ti_{50-x}Ni_{50+x}$ and $Ti_{50}(Pd_{50-x}Cr_x)$ [10], and it is unclear how general such a glassy phenomenon can be.

In general, a system tends to transforms into a glassy state rather than a long-range ordered one when there exist random defects and frustration [11]. The most common glasses are cluster spin glass [12–18] in ferromagnetic systems and relaxor [19–24] in ferroelectric systems, which possess frozen local magnetic order and frozen local ferroelectric order, respectively. They are both due to the existence of point defects, which destroy the long-range ordering of magnetic moments or electric dipoles [25]. Strain glass, which has a local order of lattice strain, is also ascribed to the introduction of point defects [8,10], which suppress the formation of long-range-ordered martensite.

* Corresponding author at: Ferroic Physics Group, National Institute for Materials Science, Tsukuba 305-0047, Ibaraki, Japan. Tel.: +81 298 59 2731; fax: +81 298 59 2701.
E-mail address: REN.Xiaobing@nims.go.jp (X. Ren).

1359-6454/$36.00
doi:10.1016/j.actamat.2010.06.019

Thus, strain glass is analogous to cluster spin glass and relaxor. Further study also reveals that strain glass shares striking similarity in physical properties with cluster spin glass and relaxor: these three physically parallel glass systems are therefore termed "ferroic glasses" [25].

Strain glass is formed by doping point defects (excess solute atoms or alloying elements) into a normal martensitic alloy. The randomly distributed point defects locally distort the crystal lattice and generate random local stresses in the system. These random local stresses dictate the local strain order and hence prohibit the formation of long-range strain-ordered martensite, although the martensite phase is favored thermodynamically. However, the local strain ordering still exists and is frozen below the freezing temperature T_0; this is the strain glass transition. Thus, in the strain glass state, there are only nanodomains with local strain-ordering. A modified Landau-type free energy landscape by considering the competition between the thermodynamic driving force and local barrier due to the existence of point defects has been proposed to understand the origin of strain glass in a phenomelogical way [25].

Among the three ferroic glasses, relaxor and cluster spin glass are known to be quite general for defect-containing ferroelectrics and ferromagnets, respectively. Thus, it is expected that strain glass should also be a quite general phenomenon in defect-containing ferroelastic/martensitic systems; however, this important implication has not been experimentally confirmed.

In the present study, in order to explore how general the strain glass is, we doped three kinds of point defects (Co, Cr, Mn) respectively into Ti–Ni to substitute for Ni. As will be seen in detail below, there is a striking similarity in the transition behavior as a function of defect doping level in all three $Ti_{50}(Ni_{50-x}D_x)$ (D = Co, Cr, Mn) systems, and the existence of the strain glass transition is confirmed in all the three systems. This implies strain glass may be a quite general phenomenon in defect-containing ferroelastic systems. Finally, it is suggested that the necessary condition for the formation of strain glass is sufficient defect doping, which can causes frustration during the ordering of strain, and this can be understood by utilizing the modified Landau-type free energy landscape for strain glass systems.

2. Experimental procedure

Base ingots of $Ti_{50}(Ni_{50-x}D_x)$ (D = Co, Cr, Mn) alloys were made by induction melting a mixture of 99.9% pure Ti, 99.9% pure Ni and 99.9% pure D in an argon atmosphere. Specimens for measurement were spark cut from the ingots. Then they were solution treated at 1273 K for 1 h in evacuated quartz tubes and quenched into ice water. In order to remove the affected surface layer, the specimens were mechanically polished, followed by chemical etching.

Differential scanning calorimetry (DSC) measurements were made with a cooling/heating rate of 10 K min^{-1} to detect the martensitic transition with exothermal/endothermic peaks as well as the transition latent heat change associated with the martensitic transition. X-ray diffraction (XRD) was used to check the possible structure change in the temperature range 143–223 K. Multifrequency dynamic mechanical analysis (DMA) was carried out to test the strain glass transition in a single cantilever mode with a constant displacement amplitude of 15 μm. The values of internal friction and elastic modulus were recorded for six frequencies (0.2, 0.4, 1, 4, 10, and 20 Hz) as a function of temperature, with a cooling and heating rate of 2 K min^{-1}.

3. Results

3.1. Evolution of transition behavior of $Ti_{50}(Ni_{50-x}D_x)$ (D = Co, Cr, Mn) alloys as a function of defect concentration x

Fig. 1 shows the transition behavior of $Ti_{50}(Ni_{50-x}D_x)$ (D = Co, Cr, Mn) alloys as a function of defect concentration x, monitored by DSC. We can see a striking similarity in the defect concentration dependence of the transition behavior, despite the difference in the defect species.

The first row of Fig. 1a1–a5 shows the variation in the transition behavior of $Ti_{50}(Ni_{50-x}Co_x)$ with defect (Co) concentration $x = 0$, 2, 4, 6, and 9 at.%; hereafter these alloys are abbreviated as 0Co, 2Co, 4Co, 6Co, 9Co, respectively. It can be seen that the pure $Ti_{50}Ni_{50}$ (0Co) alloy undergoes a B2–B19′ martensitic transition. With an increase in Co concentration to 2 at.%, 2Co first transforms into R-phase and then transforms into B19′ martensite with further cooling. Increasing the Co concentration to 4Co does not alter this two-stage B2–R–B19′ transition but simply shifts the transition temperatures R_s and M_s to lower temperatures. Further increasing the Co concentration to 6Co suppresses the second stage R–B19′ transition and 6Co undergoes only one stage B2–R transition with R_s being further decreased. However, for 9Co there appears no signature of any martensitic transition, as the DSC peak vanishes. The possibility that the martensitic transition might occur at a lower temperature beyond our DSC temperature window has been excluded by monitoring the electrical resistivity down to 10 K, confirming that 9Co indeed does not transform into normal martensite.

The second row of Fig. 1b1–b5 shows the variation in the transition behavior of $Ti_{50}(Ni_{50-x}Cr_x)$ with defect (Cr) concentration $x = 0$, 1, 2, 3 and 4.5 at.%. The Cr-doped Ti–Ni alloys show transition behavior very similar to that of the Co-doped ones. Both 1Cr and 2Cr undergo a two-stage B2–R–B19′ transition, but the R_s and M_s decrease drastically with increasing Cr concentration. 3Cr undergoes only one-step B2–R transition and R_s is further decreased compared with that of 2Cr. For 4.5Cr, however, there appears no martensitic transition, which is similar as that of 9Co.

The third row of Fig. 1c1–c5 shows the transition behavior of $Ti_{50}(Ni_{50-x}Mn_x)$ as Mn doping increases

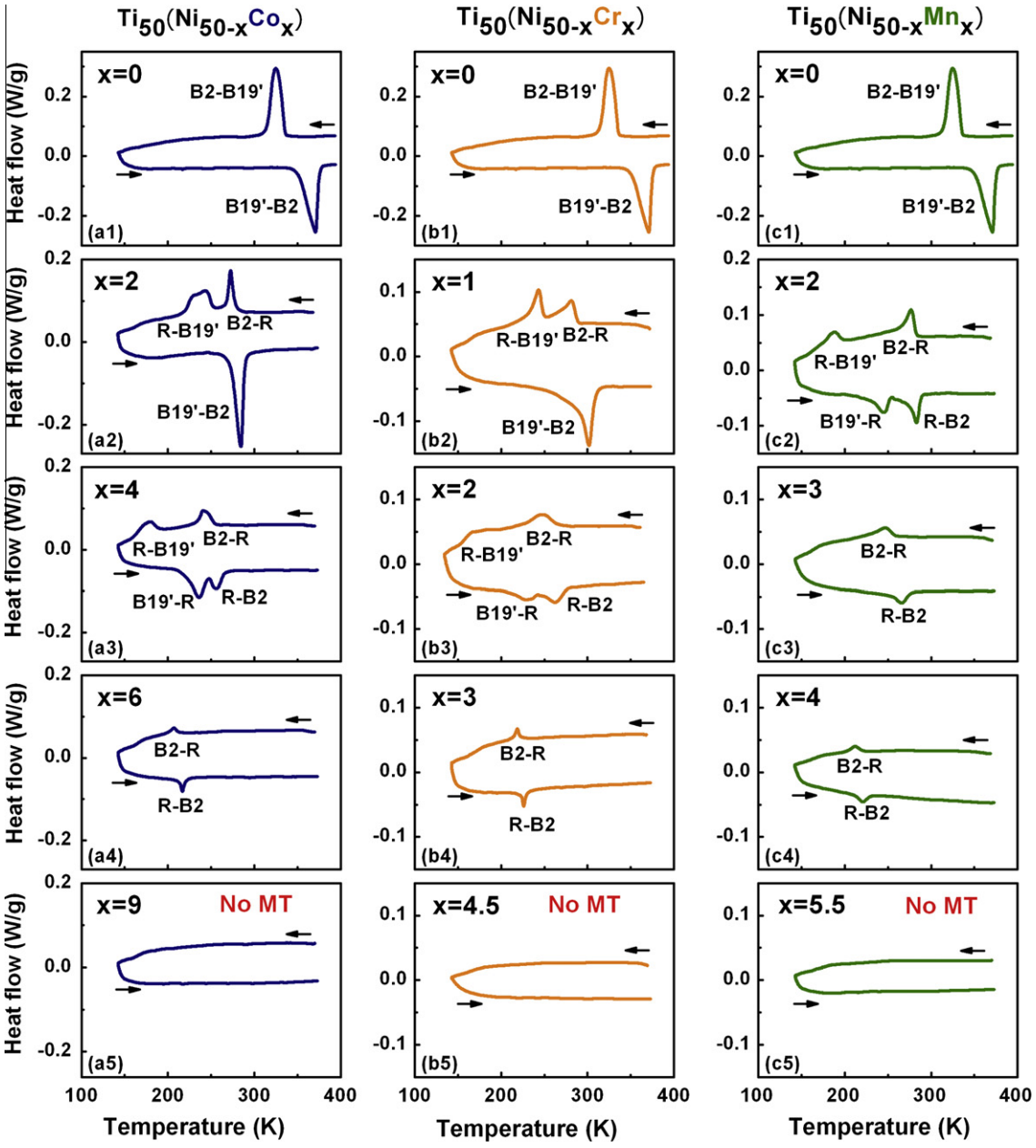

Fig. 1. The transition behavior of $Ti_{50}(Ni_{50-x}D_x)$ (D = Co, Cr, Mn) alloys as a function of defect concentration x.

from 0Mn, 2Mn, 3Mn, 4Mn to 5.5Mn. 2Mn undergoes a two-stage B2–R–B19′ two-step martenstic transition and 3Mn undergoes only a one-step B2–R transition, the R_s of which is much lower than that of 2Mn. 4Mn also shows a B2–R transition and R_s is further decreased. However, 5.5Mn does not show any signature of martensitic transition.

Fig. 2a–c shows the variation in R_s, M_s and latent heat change Q_R and Q_M (corresponding to B2–R and R–B19′ transition, respectively) with the concentration x of the three defect species Co, Cr, Mn. We can see clearly two strikingly similar features of defect doping, despite the difference in defect/dopant species: (i) a sharp decrease in R_s and M_s, and the disappearance of the martensitic transition at $x > x_c$; (ii) a drastic lowering of the transition latent heat Q_R, Q_M and the eventual disappearance at $x > x_c$. Therefore, there exists a crossover at $x = x_c$ (~9Co, ~4.5Cr, ~5.5Mn) at which the normal martensitic transition "vanishes". Such evolution with increasing defect concentration is similar to that of $Ti_{50-x}Ni_{50+x}$ and $Ti_{50}(Pd_{50-x}Cr_x)$ alloys [10,26].

We note that the dependence of M_s/R_s in the transforming compositions of these three systems is consistent with the early report by Honma [27]. Nevertheless, our interest lies more in the "non-transforming" compositions, as will be described below.

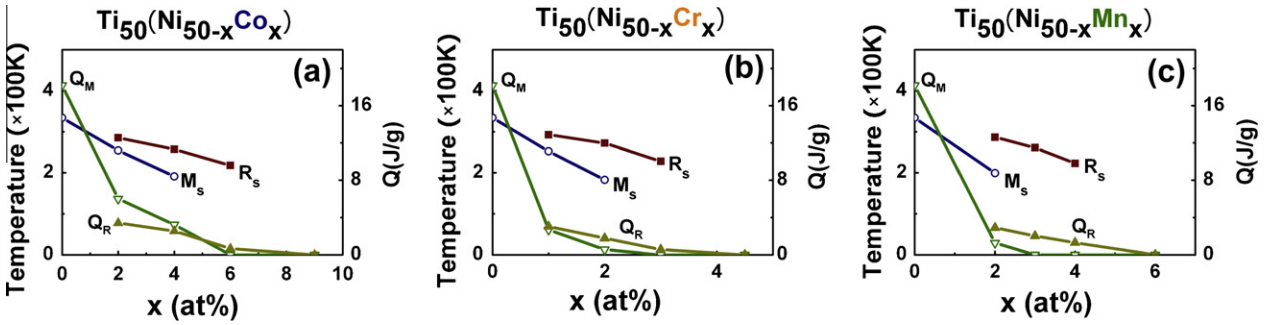

Fig. 2. M_s, R_s, Q_M, Q_R of $Ti_{50}(Ni_{50-x}D_x)$ (D = Co, Cr, Mn) alloys as a function of defect concentration x. R_s, M_s denote the onset temperatures of the B2–R and R–B19′ transition on cooling and Q_R, Q_M are the associated latent heats, respectively.

3.2. Evidence for strain glass transition in defect-doped $Ti_{50}(Ni_{50-x}D_x)$ (D = Co, Cr, Mn) alloys at $x > x_c$

For a doping level above a critical concentration x_c (~9Co, ~4.5Cr and ~5.5Mn), the DSC results in Fig. 1(a5, b5, and c5) seem to suggest that these alloys are non-transforming. However, we show in the following that they are actually not "dead" metals, but undergo a strain glass transition.

A glass transition has two essential signatures. The first signature is that it is a dynamic freezing transition from a dynamically disordered state to a frozen disordered state [11,13,14]. The corresponding dynamic freezing transition of strain glass can be identified by the frequency dispersion of the AC mechanical anomalies, which obeys the Vogel–Fulcher relation $\omega = \omega_0 \exp[-E_a/k_B(T_g(\omega) - T_0)]$ [8], where E_a is the activation barrier; $T_g(\omega)$ is the glass transition temperature measured at a frequency ω; and T_0 is the ideal glass transition temperature at 0 Hz. The second signature is that there is no macroscopic symmetry change during a glass transition; thus glass has the same average structure as its corresponding high-temperature phase, which is very different from a symmetry-breaking transition. In situ XRD investigation over a wide temperature range spanning the dynamic freezing process was employed to verify that there is no change in average structure during a strain glass transition. In the following we show the evidence for a strain glass transition for 9Co, 4.5Cr and 5.5Mn by detecting the two essential signatures.

Fig. 3a shows the transition behavior of 9Co characterized by DMA and in situ XRD investigation. We can see that the elastic modulus shows a dip and the internal friction shows a peak, both of which shift to high temperature with increasing frequency. The internal friction peak temperature $T_g(\omega)$ shifts from 167.8 to 176.8 K with frequency change from 0.2 to 20 Hz. The $\ln\omega$ vs. $T_g(\omega)$ relation follows the Vogel–Fulcher relationship shown in the inset (a0). The best fitting gives $E_a = 0.012$ eV, $\omega_0 \sim 10^4$ s^{-1}, the ideal freezing temperature $T_0 \sim 155$ K and $T_g/T_0 \sim 1.1$. The above DMA results suggest that 9Co undergoes a dynamic freezing process on cooling, which is the first signature of the strain glass. Insets (a1), (a2) and (a3) show the in situ XRD results spanning the temperature range of the above dynamic freezing process. We can see that the B2 peak persists from 223 to 143 K and there is no change in average structure, which is the second signature of a strain glass transition. Thus, from the above two essential signatures we can conclude that the seemingly "non-transforming" 9Co, as seen by DSC, actually undergoes a strain glass transition.

DMA and the in situ XRD result of 4.5Cr is shown in Fig. 3b. It can be seen clearly that the elastic modulus shows a frequency-dependent dip and the internal friction shows a frequency-dependent peak, denoted as $T_g(\omega)$, which shifts from 152 K (0.2 Hz) to 172 K (20 Hz). Ln ω vs. $T_g(\omega)$ can also be fitted by the Vogel–Fulcher relationship shown in the inset (b0) and the best fitting gives $E_a = 0.016$ eV, $\omega_0 \sim 10^4$ s^{-1}, $T_0 \sim 132$ K and $T_g/T_0 \sim 1.2$. The in situ XRD results shown in insets (b1), (b2) and (b3) show that the B2 cubic structure is maintained from 223 K to 143 K and there is no macroscopic symmetry change throughout the above dynamic freezing process. The above results confirm that 4.5Cr also undergoes a strain glass transition, like 9Co.

Similarly, Fig. 3c shows the two signatures of a strain glass transition for 5.5Mn. The elastic modulus shows a frequency dispersive dip and the internal friction shows a frequency-dependent peak from 156 K (0.2 Hz) to 170 K (20 Hz). The Vogel–Fulcher fitting between $\ln\omega$ and $T_g(\omega)$ in inset (c0) gives $E_a = 0.008$ eV, $\omega_0 \sim 10^3$ s^{-1}, $T_0 \sim 145$ K, and $T_g/T_0 \sim 1.1$. XRD results (c1), (c2) and (c3) show that the average structure is B2 cubic from 223 to 143 K. Thus, the above results also characterize the occurrence of a strain glass transition for 5.5Mn.

From the above, we have seen a common phenomenon that when defect doping is beyond a critical level x_c (~9Co, ~4.5Cr and ~5.5Mn), normal martensitic transition is suppressed; instead, such alloys undergo strain glass transition. This is similar with the case in Ni-rich $Ti_{50-x}Ni_{50+x}$ alloys when $x > 1.5$ at.% and $Ti_{50}(Pd_{50-x}Cr_x)$ alloys when $x > 9$ at.% [10,26].

3.3. Strikingly similar strain glass phase diagrams for different defect-containing ferroelastic systems

From the experimental results presented above, we obtained temperature vs. defect-concentration phase diagrams of $Ti_{50}(Ni_{50-x}D_x)$ (D = Co, Cr, Mn), as shown in

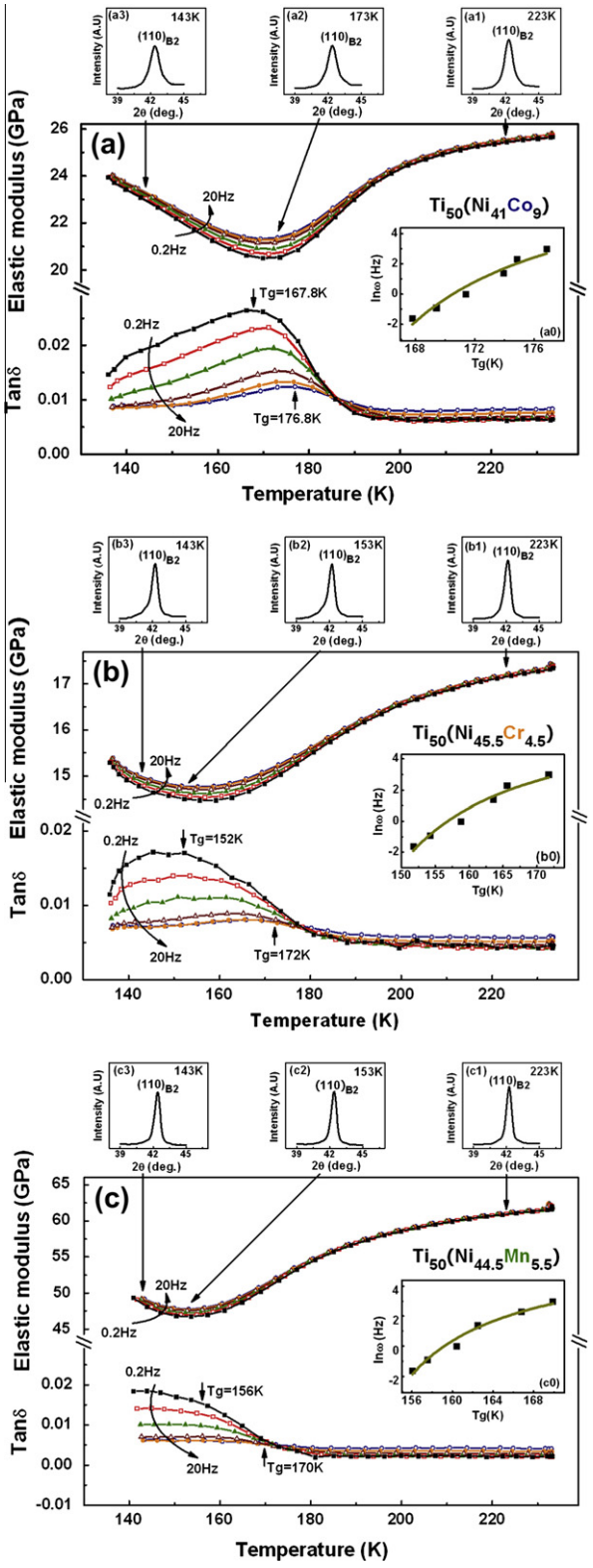

Fig. 3. Evidence for a strain glass transition for $x = 9$Co (a), $x = 4.5$Cr (b), $x = 5.5$Mn (c). DMA results show frequency (ω) dispersion in elastic modulus dip temperature and in internal friction peak temperature T_g. Ln ω vs. $T_g(\omega)$ follows the Vogel–Fulcher relationship, shown in inset (a0), (b0) and (c0), respectively. Insets (a1–a3), (b1–b3) and (c1–c3) show that the B2 peak of the parent phase does not split from 223 to 143 K, spanning the above freezing process in these alloys.

Fig. 4a–c, respectively. We can see that the three phase diagrams show the same tendency: with increasing defect concentration, the martensitic transition path changes in the following way: B2–B19′ → B2–R–B19′ → B2–R and the corresponding transition temperatures (M_s and R_s) decrease sharply for $x < 9$ at.% Co, $x < 4.5$ at.% Cr and $x < 5.5$ at.% Mn. Above a critical defect concentration x_c (~9Co, ~4.5Cr and ~5.5Mn), the normal martensitic transition is suppressed and the strain glass (STG) regime appears. Recently, more evidence for strain glass has been found in very different systems, such as the $Ti_{50}(Pd_{50-x}Cr_x)$ system [10] and even in ferroelastic ceramics [28]. These facts, together with our present findings in a series of Ti–Ni-based alloys, strongly indicate that strain glass is a general phenomenon in defect-containing ferroelastic systems. This is analogous with the other two classes of ferroic glasses: cluster spin glass in ferromagnetic systems and relaxor in ferroelectric systems.

4. Discussions

4.1. Necessary condition for the formation of strain glass: the defect concentration exceeds a critical value ($x > x_c$)

We now explore the necessary condition for the formation of strain glass, since it seems quite a general phenomenon in defect-containing ferroelastic systems. From Fig. 4, we can see a commonality in the formation of strain glass: strain glass transition occurs only when the defect concentration x exceeds a critical value x_c. Thus, it appears that sufficient defect concentration is a necessary condition for the formation of strain glass. This can be understood by considering the effect of defects on the competition between the thermodynamic driving force to form long-range strain order (martensite) and the local barrier due to the random stresses of point defects, which tends to destroy long-range order but favors short-range order [25].

Following the approach in Ref. [25], we consider the free energy landscape for a ferroelastic system at three different point doping levels: $x = 0$, $x < x_c$, $x > x_c$. Co, Cr and Mn doping produces two effects: one is to lower the thermodynamic driving force for long-range-ordered martensite, as can be seen from the lowering of R_s/M_s with increasing defect concentration; the other is to create local barriers due to the local stresses caused by random point defects. These two effects have been taken into account into the modified Landau-type free energy landscape in Ref. [25], and hence here we will utilize it to explain the defect concentration dependence of the transition behavior.

First we consider a system without point defects ($x = 0$). The free energy landscape during cooling is shown in Fig. 5a1–a3. It is characterized by the existence of two types of energy valleys: one is for the parent phase with zero strain; the other is for the martensite with a non-zero strain order (a long-range ordering of lattice deformation).

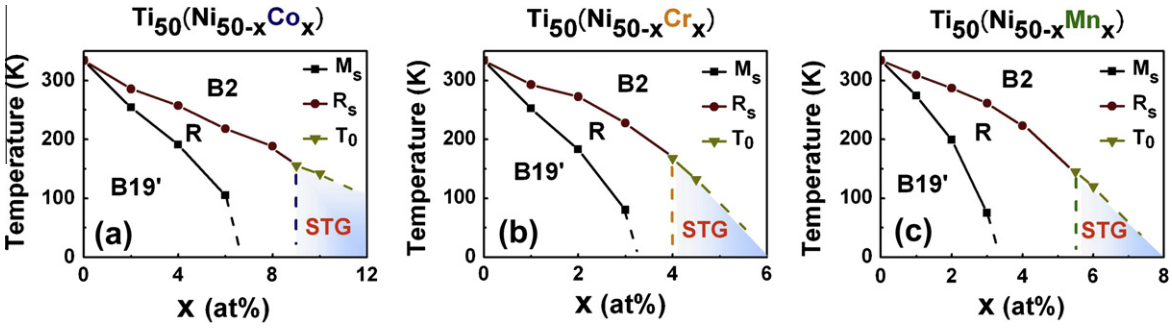

Fig. 4. Temperature (T) vs. defect concentration (x) phase diagram of $Ti_{50}(Ni_{50-x}D_x)$ (D = Co, Cr, Mn) alloys. The three phase diagrams show a similar tendency: with increasing defect concentration, the martensitic transition temperatures (M_s and R_s) decrease sharply below a critical defect concentration x_c (~9Co, ~4.5Cr and ~5.5 at.% Mn). At $x > x_c$, the martensitic transition is suppressed and strain glass regime appears. R_s/M_s represents the onset temperature of the B2–R/R–B19′ transition, respectively; T_0 is the ideal freezing temperature of strain glass at 0 Hz.

There exists a critical temperature T_a^*, at which the free energy of martensitic valley is equal to that of the parent phase, shown in (a2). At $T > T_a^*$, shown in (a1), the martensitic valley is metastable; at $T < T_a^*$, the martensitic valley is more stable than that of the parent phase, as circled in (a3). Martensitic transition occurs at a temperature $M_s < T_a^*$ due to the energy barrier between the two phases.

Fig. 5b1–b4 shows the free energy landscape for system with low-level point defects ($x < x_c$). Since the defect concentration is low, the local barrier is small. Therefore, when reaching the critical temperature T_b^*, at which the free energy of martensite is equal to that of the parent phase, the thermal activation energy k_BT is still high enough to overcome the local barrier (dotted line), as shown in (b3). Thus, the system can still transform into the long-range strain-ordered martensite despite the local barrier. However, because the thermodynamic driving force for martensite is lowered, the corresponding critical temperature T_b^* is lowered. Following the same reasoning, further increasing point defects will cause a further decrease in martensitic transition temperature, which is consistent with phase diagram shown in Fig. 4.

When point defect concentration is above a critical concentration ($x > x_c$), a fundamentally different situation appears: normal martensitic transition is suppressed and strain glass occurs. The corresponding free energy landscape during cooling from high temperature is shown in Fig. 5c1–c6. Because of the high point defect concentration, the thermodynamic driving force for martensite is significantly lowered and the local barrier becomes very large. Before the system reaches the martensitic instability temperature T_c^* (c5), the thermal activation energy K_BT becomes lower than the local barrier. As a result, the system cannot transform into normal martensite, but freezes into a glassy state at T_0, i.e. strain glass state (c4). With further cooling, the local barrier is even higher and the system is trapped in the strain glass state, although martensite is thermodynamically favored, as shown in (c6).

Thus, with the increase in defect concentration, initially the martensitic transition temperature is decreased but normal martensite is still maintained. However, when the defect concentration exceeds a critical value x_c, prior to the martensitic instability at T_c^*, the system is frozen into a strain glass at $T_0 > T_c^*$, as shown in (d). Therefore, the formation of strain glass results from the competition between the thermodynamic driving force toward martensite and the local barrier. The latter dominates at $x > x_c$ and the system transforms into a frozen disordered state, strain glass, instead of undergoing a long-range strain-ordering, martensitic transition.

4.2. The exceptional case of TiNi–Pd/Pt/Au: the opposite effect of point defect on the thermodynamic driving force toward long-range strain order (martensite)

As discussed above, strain glass seems to be a general phenomenon in defect-containing ferroelastic systems. However, it should be noted that not all kinds of point defects can lead to a strain glass at high doping level. The best known examples are Pd/Pt/Au-doped Ti–Ni-based alloys [29–31], where normal martensitic transition occurs over the whole doping range.

We now show that there is actually no contradiction with the above analysis. The "exceptions" are simply due to an opposite effect of these defects on the thermodynamic stability of martensite.

Being different from Co, Cr, and Mn, which lower martensite stability (as seen from the decrease of R_s/M_s with x in Fig. 4), Pd/Pt/Au doping increases the martensite stability, as can be seen from the increase of M_s with increasing x [29–31]. This difference is responsible for the non-existence of strain glass in Pd/Pt/Au-doped Ti–Ni alloys. In the case of Co/Cr/Mn doping, the two effects of point defects, i.e. changing thermodynamic driving force toward martensite and favoring short-range order due to the local random stresses, are in the same direction. As explained above, both disfavor a long-range ordering and favor a local ordering (Fig. 5). However, for Pd/Pt/Au, the two effects act in the opposite direction, as schematically shown in Fig. 6. Fig. 6a1–a4 describe the free energy landscape on cooling for the $Ti_{50}Ni_{50}$ alloy without any point defect. At a critical temperature T_1^* (a3), the free energy of the

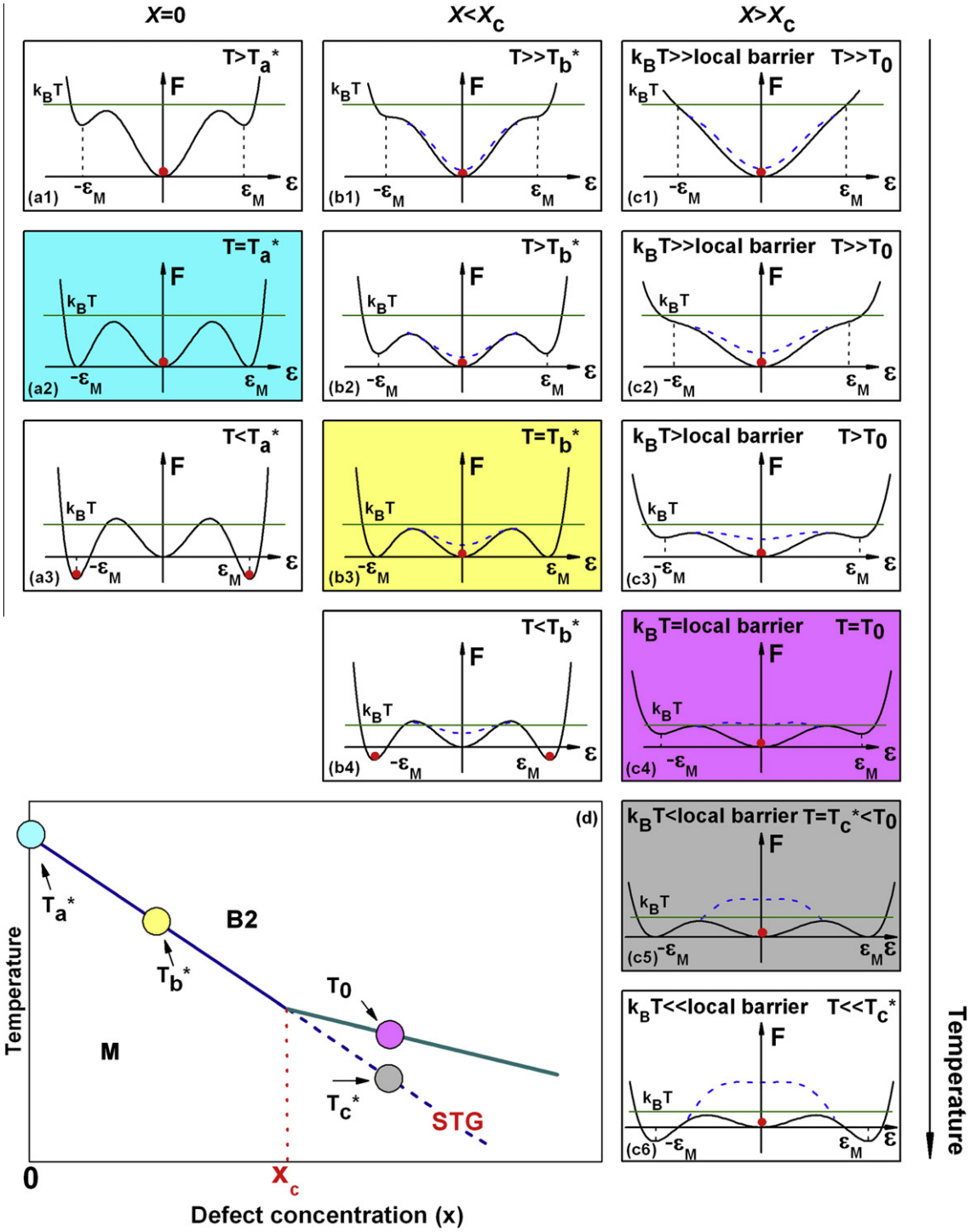

Fig. 5. The free energy landscape for the Co/Cr/Mn-doped Ti–Ni-based systems with point defect concentration $x = 0$, $x < x_c$, $x > x_c$, as a function of decreasing temperature. The difference between the dashed line and the bottom line represents the local barrier due to the local strain (see Ref. [25] for a detailed explanation); k_BT represents the thermal activation energy; T_a^*, T_b^*, T_c^* represent the thermodynamic instability temperature (i.e. $F_{\text{parent}} = F_{\text{martensite}}$) of the parent phase for $x = 0$, $x < x_c$, $x > x_c$ respectively; T_0 represents the ideal freezing temperature of the strain glass transition for the system with $x > x_c$. The red point represents the stable state of the system. When $x < x_c$, the local barrier is low and thermal activation k_BT at T_b^* is sufficient to overcome the barrier, so normal martensite can be formed, but the martensitic transition temperature is sharply decreased. When $x > x_c$, the local barrier is so high that k_BT is not high enough to overcome it, so the system is frozen in a glassy state, and martensitic transition is completely suppressed. Thus, $T_c^* < T_0 < T_b^* < T_a^*$, as can be seen in the schematic phase diagram in (d). (For interpretation of the references to colour in this figure legend, the reader is referred to the web version of this article.)

martensitic valley is equal to that of the parent phase. The martensitic transition occurs at a temperature $M_{s1} < T_1^*$ due to the energy barrier between the two phases. With Pd/Pt/Au doping, shown in Fig. 6b1–b3, the thermody-

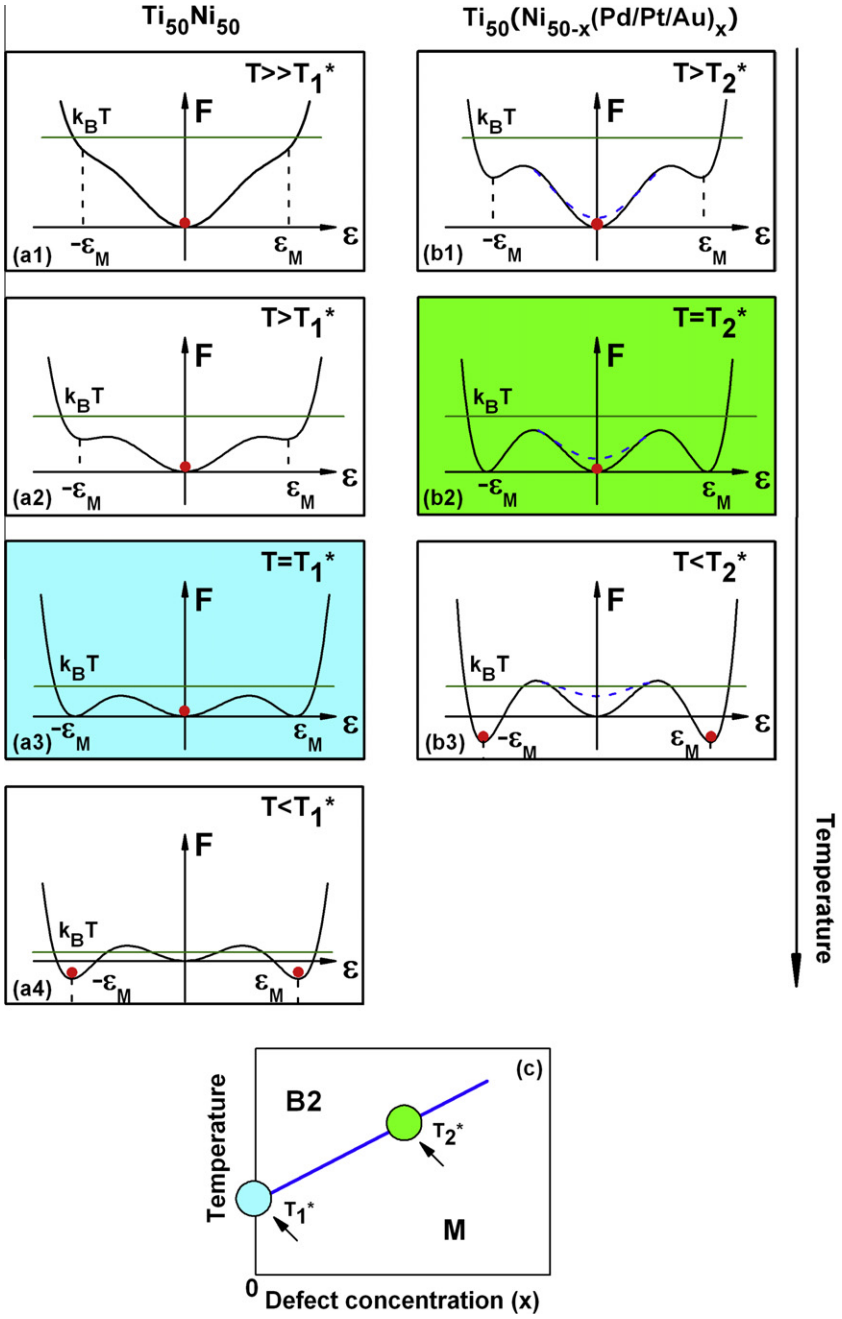

Fig. 6. The free energy landscape for the Pd/Pt/Au-doped Ti–Ni-based system with point defect concentration $x = 0$, $x > 0$, as a function of decreasing temperature. The difference between the dashed line and the bottom line represents the local barrier due to the local strain; k_BT represents the thermal activation energy; T_1^*, T_2^* represent the critical temperature at which the free energy of martensite is equal to that of the parent phase for $x = 0$, $x > 0$, respectively. The red point represents the stable state of the system. (For interpretation of the references to colour in this figure legend, the reader is referred to the web version of this article.)

namic stability of martensite is increased, so at a temperature T_2^* higher than T_1^*, the free energy of the martensitic valley can be equal to that of the parent phase (b2). Thus, the system can transforms into martensite at temperature $M_{s2} > M_{s1}$, although there also exists a local barrier due to the random local stress. Therefore, Pd/Pt/Au doping increases the thermodynamic driving force for long-range strain-ordering and thus favors martensite formation; this effect surpasses the local ordering tendency caused by the random point defects. As a result, the system remains martensitic without going to strain glass.

Therefore, the contrasting transition behavior between Co/Cr/Mn-doped Ti–Ni alloys and Pd/Pt/Au-doped Ti–Ni alloys suggests that if doping point defects can simultaneously decrease the martensite stability and favor the local ordering, then a strain glass transition occurs at $x > x_c$, as

is the case in Co/Cr/Mn-doped Ti–Ni alloys. However, if one of the two conditions is not satisfied (as occurs in Pd/Pt/Au-doped Ti–Ni alloys), strain glass cannot be achieved.

It is notable that a recent theoretical model has successfully reproduced many important features of strain glass [32]. However, the theory predicts that strain glass can form even in systems where point defects increase the M_s temperature. This seems at variance with the experimental results of TiNi–Pd/Pt/Au, where point defects cause an increase in M_s and there is no strain glass in these systems. The discrepancy between simulation and experimental results needs further investigation.

4.3. Understanding the evolution of transition latent heat with increasing defect concentration x

As shown in Fig. 2, at low doping level ($x < x_c$), the transition latent heat (or entropy) decreases with increasing defect concentration; at high doping level ($x > x_c$), the transition latent heat becomes almost zero. Such evolution can be understood by the modified free energy landscape shown in Fig. 5.

The transition entropy is proportional to the change in strain order between the parent phase and martensite phase at the transition temperature [33]. For the pure $Ti_{50}Ni_{50}$ alloy, there is no local strain due to the point defects, so the transition is from a fully strain-disordered parent state (a1) to a fully long-range strain-ordered martensite state (a3): thus the change of strain order is the largest and the transition entropy is the largest, as shown in Fig. 2. For low level-doped alloys ($x < x_c$), there is some local strain due to the random point defects, and the transition is between a partially strain-disordered (locally ordered) parent phase (b2) and an imperfectly long-range strain-ordered martensite (b4); thus the change in strain order and the transition entropy becomes less. With increasing defect doping, more local strains are created by random point defects, so the parent phase is partially disordered with more local ordered strain and the long-range strain-ordered martensite phase becomes more imperfect. Thus, the change in strain order becomes less and the entropy change becomes smaller, which is consistent with Fig. 2. At high defect content ($x > x_c$), the martensite transition is completely suppressed and strain glass transition occurs. Thus, the parent phase is a disordered state with local ordered strain (c3) and the strain glass state is a frozen glassy state with local ordered strain (c5). As a result, there is no obvious change in the degree of strain order (or no symmetry breaking) during strain glass transition, and the transition entropy or latent heat becomes nearly zero in the strain glass regime, as shown in Fig. 2.

5. Conclusions

In order to check whether or not strain glass is a general phenomenon, as well as the necessary condition for the occurrence of strain glass, we systematically studied the transition behavior of three different systems $Ti_{50}(Ni_{50-x}D_x)$ (D = Co, Cr, Mn) as a function of point defect concentration x. We found that there is a striking similarity in the transition behavior as a function of doping level of D in all $Ti_{50}(Ni_{50-x}D_x)$ (D = Co, Cr, Mn) alloys. The main conclusions are summarized as follows:

(1) At low-level doping ($x < x_c$), all the alloys show a normal martensitic transition. With increasing defect concentration, the martensitic transition path changes in the following way: B2–B19′ → B2–R–B19′ → B2–R. Meanwhile, both the martensitic transition temperature (R_s and M_s) and the latent heat (Q_R, Q_M) associated with the martensitic transition decrease with increasing x.
(2) With doping level exceeding a critical value ($x > x_c$), the normal martensitic transition is completely suppressed and the transition latent heat disappears. Instead, they all undergo a strikingly similar strain glass transition.
(3) The existence of strain glass in these three different defect-doped $Ti_{50}(Ni_{50-x}D_x)$ (D = Co, Cr, Mn) alloys and in the reported Ni-rich Ti–Ni and Cr-doped TiPd alloys clearly suggests that strain glass may be a quite general phenomenon in defect-containing ferroelastic systems. This is analogous to cluster spin glass in ferromagnetic systems and relaxor in ferroelectric systems.
(4) The necessary condition for the formation of strain glass is that the defect concentration exceeds a critical value; but this is not a sufficient condition. To create a strain glass, a dopant should also destabilize the stability of normal martensite. This can be understood in a phenomelogical way by a modified Landau-type free energy landscape.
(5) The evolution of transition temperature (R_s and M_s) and the latent heat (Q_R, Q_M) as a function of defect concentration also can be well explained by a modified Landau-type free energy landscape.

Acknowledgements

The authors gratefully acknowledge the support of National Natural Science Foundation of China (Grant No. 50720145101 and No. 50771079), National Basic Research Program of China (Grant No. 2010CB631003), as well as NCET and the 111 project of China (B06025).

References

[1] Otsuka K, Ren X. Prog Mater Sci 2005;50:511.
[2] Otsuka K, Wayman CM, editors. Shape memory materials. Cambridge: Cambridge University Press; 1998.
[3] Otsuka K, Kakeshita T. MRS Bull; 2002.
[4] Khachaturyan AG. Theory of structural transition in solids. New York: Wiley; 1983.

[5] Salje EKH. Phase transition in ferroelastic and Co-elastic crystal. Cambridge: Cambridge University Press; 1993.
[6] Lashley JC, Shapiro SM, Winn BL, Opeil CP, Manley ME, Alatas A, et al. Phys Rev Lett 2008;101:135703.
[7] Planes A, Manosa L, Acet M. J Phys: Condens Matter 2009;21:233201.
[8] Sarkar S, Ren X, Otsuka K. Phys Rev Lett 2005;95:205702.
[9] Wang Y, Ren X, Otsuka K. Phys Rev Lett 2006;97:225703.
[10] Zhou YM, Xue DZ, Ding XD, Otsuka K, Sun J, Ren XB. Appl Phys Lett 2009;95:151906.
[11] Binder K. Glassy materials and disordered solids. London: World Scientific; 2005.
[12] Sherrington D, Kirkpatrick S. Phys Rev Lett 1975;35:1792.
[13] Mydosh JA. Spin glasses. London: Taylor & Francis; 1993.
[14] Fischer KH, Hertz JA. Spin glasses. Cambridge: Cambridge University Press; 1991.
[15] Binder K, Young AP. Rev Mod Phys 1986;58:801.
[16] Snyder J, Slusky JS, Cava RJ, Schiffer JR. Nature 2001;413:48.
[17] Beck PA. Phys Rev Lett 1983;50:1021.
[18] Rakers LD, Beck PA. Phys Rev B 1988;38:7002.
[19] Viehland D, Li JF, Jang SJ, Cross LE, Wuttig M. Phys Rev B 1992;46:8013.
[20] Semenovskaya S, Khachaturyan AG. Ferroelectrics 1998;206–207:157.
[21] Vugmeister BE, Glinchuk MD. Rev Mod Phys 1990;62:993.
[22] Semenovskaya S, Khachaturyan AG. J Appl Phys 1998;83:5125.
[23] Samara GA. J Phys: Condens Matter 2003;15:R367.
[24] Viehland D, Jang SJ, Cross LE, Wuttig M. J Appl Phys 1990;68:2916.
[25] Wang Y, Ren X, Otsuka K, Saxena A. Acta Mater 2008;56:2885.
[26] Zhang Z, Wang Y, Wang D, Zhou YM, Otsuka K, Ren XB. Phys Rev B 2010;81:224102.
[27] Honma T. In: Funakubo H, editor. Shape memory alloys. New York: Gordon & Breach; 1987.
[28] Zhang P, BS thesis, Xi'an Jiaotong University; 2009.
[29] Nam TH, Saburi T, Shimizu K. Trans JIM 1990;31:959.
[30] Otsuka K, Golberg D. In: Vincenzini S, editor. Intelligent matter and systems. Techna Srl; 1995.
[31] Matveeva NM, Khachin VN, Shivokha VP. In: Drits ME, editor. Stable and metastable phase equilibrium in metallic systems. Moscow: Nauka; 1985.
[32] Vasseur R, Lookman T. Phys Rev B 2010;81:094107.
[33] Careri G. Order and disorder in matter. Reading, MA: Addison-Wesley; 1984.